Materials Today Chemistry 12 (2019) 61–70

Contents lists available at ScienceDirect

Materials Today Chemistry

journal homepage: www.journals.elsevier.com/materials-today-chemistry/

Cryopreserved cell-laden alginate microgel bioink for 3D bioprinting of living tissues

O. Jeon [a], Y.B. Lee [a], T.J. Hinton [b], A.W. Feinberg [b, c], E. Alsberg [a, d, *]

[a] Department of Biomedical Engineering, Case Western Reserve University, USA
[b] Department of Biomedical Engineering, Carnegie Mellon University, USA
[c] Department of Materials Science & Engineering, Carnegie Mellon University, USA
[d] Department of Orthopaedic Surgery, Case Western Reserve University, USA

ARTICLE INFO

Article history:
Received 27 September 2018
Accepted 21 November 2018
Available online 14 January 2019

Keywords:
Tissue engineering
Microscale hydrogel
Bone
Cartilage

ABSTRACT

Cell-laden microgels have been used as tissue building blocks to create three-dimensional (3D) tissues and organs. However, traditional assembly methods cannot be used to fabricate functional tissue constructs with biomechanical and structural complexity. In this study, we present directed assembly of cell-laden dual-crosslinkable alginate microgels that comprised oxidized and methacrylated alginate (OMA). Cell-laden OMA microgels can be directly assembled into well-defined 3D shapes and structures under low-level ultraviolet light. Stem cell–laden OMA microgels can be successfully cryopreserved for long-term storage and on-demand applications, and the recovered encapsulated cells maintained equivalent viability and functionality to the freshly processed stem cells. Finally, we have successfully demonstrated that cell-laden microgels can be assembled into complicated 3D tissue structures via freeform reversible embedding of suspended hydrogels (FRESH) 3D bioprinting. This highly innovative bottom-up strategy using FRESH 3D bioprinting of cell-laden OMA microgels, which are cryopreservable, provides a powerful and highly scalable tool for fabrication of customized and biomimetic 3D tissue constructs.

1. Introduction

Living tissues are ensembles of modular building blocks that organize into hierarchical structures across multiple length scales from microns to meters. During the course of their development, these modules of cells and extracellular components arrange in well-defined three-dimensional (3D) microarchitectures to establish proper coordination of cell–cell and cell–extracellular matrix (ECM) interactions and generate tissue-specific function [1–3]. Therefore, in context of tissue engineering, recreating the spatial organization of these modules may be necessary to build a functional tissue construct that can be used therapeutically. Conventional tissue engineering methods use a 'top-down' approach in which cells are seeded on or within a biodegradable scaffold and exposed to cues such as biochemical signals and mechanical stimulation to guide the formation of appropriate tissue organization (i.e. the relative spatial positions of its cellular and ECM components) and architecture (i.e. its 3D structure/geometry) [4,5]. However, the top-down approach still faces challenges such as precisely positioning cells of multiple types, achieving tissue-specific geometries and cell densities, and incorporating vasculature throughout the 3D space of the tissue constructs [6–9]. To address these issues, 'bottom-up' strategies are emerging as alternative means for functional tissue engineering. Distinct from the top-down approach, the bottom-up method involves starting with simplified building blocks composed of cells, materials, and/or bioactive factors and assembling them into larger, complex tissues that have organization and architecture necessary for functionality [10,11]. It is possible to engineer the individual blocks in various shapes and sizes with desired types of cells or combinations of cells and materials, and then assemble them manually into an ensemble during the scale-up process [11–13]. This modularity allows enhanced control over the relative spatial arrangement of cells, ECM, and/or bioactive factors during the tissue construction, making it possible to engineer sophisticated architectures that mimic the native tissues.

Microscale hydrogels (microgels) are frequently used as building blocks for bottom-up tissue engineering [7]. They exhibit

* Corresponding author. Department of Biomedical Engineering, Case Western Reserve University, USA.
E-mail address: eben.alsberg@cwru.edu (E. Alsberg).

https://doi.org/10.1016/j.mtchem.2018.11.009
2468-5194/

properties similar to those of bulk hydrogels that have been used extensively in previous biomedical applications, such as tunable physical properties, cell adhesivity, and biodegradability [14,15]. To date, numerous reports have demonstrated assembly of cell-laden microgels, such as endothelial cell–laden microgels randomly assembled into microvasculature-like constructs [16], cell-encapsulated microgels micromolded into defined shapes and sizes for self-assembly [17], and cell-containing microgels directly assembled by microfluidic channels [18,19], hydrophobic–hydrophilic interactions [20], or acoustic waves [21]. Random assembly approaches of cell-laden microgels can be used to scale up and form bulk structures, but they lack control over the spatial arrangement of the microgels [16]. In contrast, manual assembly of microgels offers control over spatial distribution of multiple cell types, but the process is relatively slow and challenging to scale up into large tissues. For example, microfluidic-directed assembly can be used to create highly intricate microgel assembly architectures, but complex equipment is required, and it is a time intensive process [22,23]. Directed-assembly by hydrophobic and hydrophilic interactions is a simple way to control the size, shape, and pattern of the architecture of the microgel ensemble, but it requires organic solvents that are cytotoxic and also suffers from poor mechanical properties of the construct after assembly [20,24]. Application of acoustic waves is a rapid and non-invasive way to assemble cell-encapsulating microgels, but it also does not allow precise control over shaping the bulk aggregates into predefined geometries [21]. Owing to the aforementioned limitations, there is need for a robust strategy that not only offers simple, quick, and scalable assembly of microgels into functional 3D tissue constructs but also assures cell viability and desired behavior after assembly.

One of the promising technologies that enables bottom-up fabrication of biological constructs is 3D bioprinting, which is a layer-by-layer additive manufacturing process that allows precise positioning of the bioinks as per spatial instructions provided by digital models [25,26]. This strategy offers simple, rapid, and controlled expansion of microgels into any complex 3D microstructure without the need of external tools or molds that are specific for each microstructure. Among the commonly used printing systems, fluid extrusion printers, which use a syringe and piston to dispense bioinks through microscale nozzles, enable printing of 3D cell-laden structures composed of high concentrations of hydrogels [27,28]. However, implementing these printers to produce large, high-resolution, and mechanically stable free-form hydrogel-based tissue constructs of desired shapes requires a bioink printing material with appropriate viscosity, structural and mechanical integrity after gelation, and cytocompatibility [25,29].

Previously, we have demonstrated that photocrosslinked oxidized methacrylated alginate (OMA) hydrogels promote enhanced cell adhesion and spreading, exhibit biodegradability that supports cell infiltration and migration, and can be formed with a wide range of mechanical properties [30]. Owing to these characteristics, we hypothesized that OMA would be ideal for generating cell-encapsulating microgels to serve as building blocks for forming larger, more complicated tissue constructs. Therefore, in this report, we have fabricated OMA microgels and explored their potential as building blocks for manual assembly and 3D printing for tissue engineering applications. OMA droplets can be ionically crosslinked into microgels with the addition of calcium ions and then assembled together into a bulk hydrogel by photocrosslinking under low-level ultraviolet (UV) light. Using these principles, we heterogeneously assembled the OMA microgels and scaled them up into large, defined, and complex biological structures using the free-form reversible embedding of suspended hydrogels (FRESH) 3D bioprinting technique [31]. To the best of our knowledge, this is the first study demonstrating the capacity to bioprint cell-encapsulated microgels, allowing for simple, rapid, scalable fabrication of tissue constructs with predefined geometrical features for regenerative medicine applications.

2. Experimental

2.1. Synthesis of OMA

Oxidized alginate (OA) was prepared by reacting sodium alginate (Protanal LF 200S, FMC Biopolymer) with sodium periodate (Sigma) using a modification of a previously described method [30,32]. Briefly, sodium alginate (10 g) was dissolved in ultrapure deionized water (diH_2O, 900 ml) overnight. Sodium periodate (0.1 g) was dissolved in 100 ml of diH_2O, added to alginate solution under stirring to achieve 1% theoretical alginate oxidation, and allowed to react in the dark at room temperature for 24 h. The OMA macromer was prepared by reacting OA with 2-aminoethyl methacrylate (AEMA; Sigma). To synthesize OMA, 2-morpholinoethanesulfonic acid (MES, 19.52 g; Sigma) and NaCl (17.53 g) were directly added to an OA solution (1 L) and the pH was adjusted to 6.5. N-hydroxysuccinimide (NHS, 1.176 g; Sigma) and 1-ethyl-3-(3-dimethylaminopropyl)-carbodiimide hydrochloride (EDC, 3.888 g; Sigma) (molar ratio of NHS:EDC = 1:2) were added to the mixture under stirring to activate 20% of the carboxylic acid groups of the alginate. After 5 min, AEMA (1.688 g) (molar ratio of NHS:EDC:AEMA = 1:2:1) was added to the product, and the reaction was maintained in the dark at room temperature for 24 h. The reaction mixture was precipitated with the addition of excess of acetone, dried in a fume hood, and rehydrated to a 1% w/v solution in diH_2O for further purification. The OMA was purified by dialysis against diH_2O (MWCO 3500; Spectrum Laboratories Inc.) for 3 days, treated with activated charcoal (5 g/L, 50–200 mesh, Fisher, Pittsburgh, PA) for 30 min, filtered (0.22 μm filter), and lyophilized. To determine the levels of alginate oxidation and methacrylation, the OMA were dissolved in deuterium oxide (D_2O, 2 w/v %), and ^{1}H-NMR spectra were recorded on a Varian Unity-300 (300 MHz) NMR spectrometer (Varian Inc.) using 3-(trimethylsilyl)propionic acid-d_4 sodium salt (0.05 w/v %) as an internal standard [30].

2.2. Fabrication and directed assembly of OMA hydrogel beads

OMA (2.5 w/v %) was dissolved in DMEM (Sigma) with a photoinitiator (2-Hydroxy-4′-(2-hydroxyethoxy)-2-methylpropiophenone, 0.05 w/v %, Sigma) at pH 7.4. OMA solution was loaded into a 5-ml syringe, and then the syringe was installed in a syringe pump (NE-1000X, New Era Pump System Inc.). The OMA solution was pumped at 0.5 ml/s, and the droplets dripped into a collection bath containing an aqueous solution of $CaCl_2$ (0.2 M) and maintained in the bath for 30 min as shown in Fig. 1a. The resultant OMA beads were collected and washed with the Dulbecco's Modified Eagle"s medium (DMEM) thrice. To fabricate magnetic microgels, iron (III) oxide nanoparticles (1 w/v %, size <50 nm; Sigma) were suspended in OMA solution before crosslinking. After manually connecting the OMA beads on a glass slide, the resulting OMA bead constructs were exposed to UV light (Omnicure® S1000, EXFO Photonic Solution Inc.) at ~ 20 mW/cm^2 for 1 min to stabilize the assembled structures. The magnetic beads were also crosslinked together under UV light at 20 mW/cm^2 for 1 min after collecting them using a permanent magnet.

2.3. hMSC-encapsulated OMA microgels

To isolate human bone marrow–derived mesenchymal stem cells (hMSCs), bone marrow aspirates were obtained from the posterior iliac crest of a healthy 23-year-old male donor under a protocol approved by the University Hospitals of Cleveland

Institutional Review Board. The aspirates were washed with a growth medium composed of low-glucose DMEM (DMEM-LG; Sigma) with 10% prescreened fetal bovine serum (FBS; Gibco). Mononuclear cells were isolated by centrifugation in a Percoll (Sigma) density gradient, and the isolated cells were plated at 1.8×10^5 cells/cm^2 in DMEM-LG containing 10% FBS and 1% penicillin/streptomycin (P/S, Thermo Fisher Scientific) in an incubator at 37 °C and 5% CO_2. After 4 days of incubation, non-adherent cells were removed, and adherent cell were maintained in DMEM-LG containing 10% FBS and 1% P/S with media changes every 3 days. After 14 days of culture, the cells were passaged at a density of 5×10^3 cells/cm^2 [33]. To fabricate hMSC-laden OMA microgels, hMSCs were expanded in growth media consisting of DMEM-LG with 10% FBS (Sigma), 1% P/S, and 10 ng/ml fibroblast growth factor-2 (FGF-2, R&D) and suspended in OMA solution (passage 3, 2×10^6 cells/ml). hMSC-suspended OMA solutions were loaded into a 3-ml syringe, and then the syringe was connected to a coaxial microdroplet generator, designed in our laboratory (Fig. 1c and Supplementary Fig. 3). The hMSC-suspended OMA solution was pumped at 0.5 ml/s with an outer air flow rate of 15 L/min, and the droplets dripped into a collection bath containing an aqueous solution of $CaCl_2$ (0.2 M). After fully ionically crosslinking the microgels in the bath for 30 min, the resultant hMSC-laden OMA microgels were collected and washed with DMEM thrice. The viability of hMSCs immediately after encapsulation in the OMA microgels was investigated using a Live/Dead assay composed of fluorescein diacetate (FDA, 1.5 mg/ml in dimethyl sulfoxide [Research Organic Inc.], Sigma) and ethidium bromide (EB, 1 mg/ml in PBS; Thermo Fisher Scientific). The staining solution was freshly prepared by mixing 1 ml of FDA solution and 0.5 ml of EB solution with 0.3 ml of PBS (pH 8). 20 μl of staining solution was added into each 1 ml of microgels suspended in DMEM and incubated for 3–5 min at room temperature, and then stained hydrogel-cell constructs were imaged using a fluorescence microscope (ECLIPSE TE 300) equipped with a digital camera (Retiga-SRV). Unstained hMSC-laden OMA microgels were transferred to 100-ml spinner flasks (Bellco Glass Inc., Vineland, NJ) containing 80 ml of growth media. The spinner flasks were placed in a humidified incubator at 37 °C with 5% CO_2 and stirred at 40 rpm. After 4 weeks of culture, the viability of encapsulated hMSCs in the OMA microgels was again evaluated using the Live/Dead assay before and after assembly of the OMA microgels as described above.

2.4. Cryopreservation of hMSC-laden OMA microgels

hMSC-laden OMA microgels that underwent cryopreservation were frozen for one month before being cultured for osteogenic and chondrogenic differentiation. The cryopreservation process was based on the following protocol: hMSC-laden OMA microgels were placed in a polypropylene cryovial (VWR) containing a solution of 10% (v/v) dimethyl sulphoxide (DMSO; Sigma) in growth media at room temperature. The samples were cooled by placing in a conventional freezer (−20 °C) for 1 h and then moved into a −80 °C freezer. After 12 h at −80 °C, samples were stored inside a liquid nitrogen tank (Statebourne Biosystem) for one month. After 1 month of cryopreservation, the hMSC-laden OMA microgels were thawed rapidly at 37 °C, and the viability of encapsulated hMSCs in the OMA microgels was investigated using the Live/Dead assay as previously described.

2.5. Osteogenic and chondrogenic differentiation of the hMSC-laden OMA microgels

The cryopreserved hMSC-laden OMA microgels were transferred to 100-ml spinner flasks (Bellco Glass Inc., Vineland, NJ) containing 80 ml of growth media. The spinner flasks were placed in a humidified incubator at 37 °C with 5% CO_2 and stirred at 40 rpm. After 2 days of culture, the medium was replaced with the osteogenic differentiation medium (10 mM β-glycerophosphate [Calbiochem], 37.5 μg/ml ascorbic acid [Wako USA], 100 nM dexamethasone [MP Biomedicals], and 100 ng/ml BMP-2 in DMEM-high glucose) containing 10% FBS and 1% P/S or the chondrogenic differentiation medium (10% ITS + Premix, 100 nM dexamethasone, 37.5 μg/ml l-ascorbic acid-2-phosphate, 1 mM sodium pyruvate, 100 μM nonessential amino acids, and 10 ng/ml TGF-β_1 in DMEM-high glucose). The osteogenic and chondrogenic media were changed twice a week. As a comparative group (fresh group), freshly made hMSC-laden OMA microgels without prior cryopreservation were cultured in spinner flasks containing osteogenic or chondrogenic differentiation media. After 4 weeks of culture, 1 ml of hMSC-laden OMA microgel suspension solution was taken from each spinner flask. After removing media, microgels were homogenized at 35,000 rpm for 30 s using a TH homogenizer (Omni International) in 1 ml of ALP lysis buffer (CelLytic™ M, Sigma). The homogenized solutions were centrifuged at 500 g with a Sorvall Legent RT Plus Centrifuge (Thermo Fisher Scientific). For ALP activity measurements, the supernatant (100 μl) was treated with *p*-nitrophenylphosphate ALP substrate (pNPP, 100 μl; Sigma) at 37 °C for 30 min, and then 0.1 N NaOH (50 μl) was added to stop the reaction. The absorbance was measured at 405 nm using a plate reader (VersaMax, Molecular Devices) (N = 3). A standard curve was made using the known concentrations of 4-nitrophenol (Sigma). DNA content in the supernatant (100 μl) was measured using a Quant-iT PicoGreen assay kit (Invitrogen) as per the manufacturer's instructions. Fluorescence intensity of the dye-conjugated DNA solution was measured using a fluorescence plate reader (FMAX, Molecular Devices) set at 485 nm excitation and 538 nm emission (N = 3). After an equal volume of 1.2 N HCl was added into each lysate solution, the mixed solutions were centrifuged at 500 g with a Sorvall Legent RT Plus Centrifuge. Calcium content of the encapsulated hMSCs was quantified using a calcium assay kit (Pointe Scientific) as per the manufacturer's instructions. Supernatant (4 μl) was mixed with a color and buffer reagent mixture (250 μl), and the absorbance was read at 570 nm on a microplate reader (VersaMax, N = 3). All ALP activity and calcium content measurements were normalized to DNA content. To visualize calcium deposition in the osteogenically differentiated microgels, they were embedded in optimal cutting temperature compound (OCT; Thermo Fisher Scientific), sectioned at a thickness of 20 μm, stained with Alizarin red S, and then imaged using a microscope (Leitz Laborlux S, Leica) equipped with a digital camera (Coolpix 995, Nikon).

After 4 weeks of culture in the chondrogenic differentiation medium, the viability and morphology of encapsulated hMSCs in the OMA microgels were examined using the Live/Dead assay. Stained microgels were imaged using a fluorescence microscope equipped with a digital camera. For glycosaminoglycan (GAG) measurement, microgels were homogenized for 60 s in papain buffer (1 mL, pH 6.5)) containing papain (25 μg/ml; Sigma), L-cysteine (2×10^{-3} M; Sigma), sodium phosphate (50×10^{-3} M), and EDTA (2×10^{-3} M). The homogenate was papain-digested at 65 °C overnight. The following day, GAG was quantified using a dimethylmethylene blue assay [34], and DNA was measured using the PicoGreen assay as described previously. To visualize the GAG distribution in the chondrogenically differentiated microgels, microgels were embedded in OCT, sectioned at a thickness of 20 μm, stained with Alcian blue and Toluidine blue O, and then imaged using a microscope equipped with a digital camera. To show the feasibility of heterogeneous assembly of the OMA microgels, osteogenically and chondrogenically differentiated

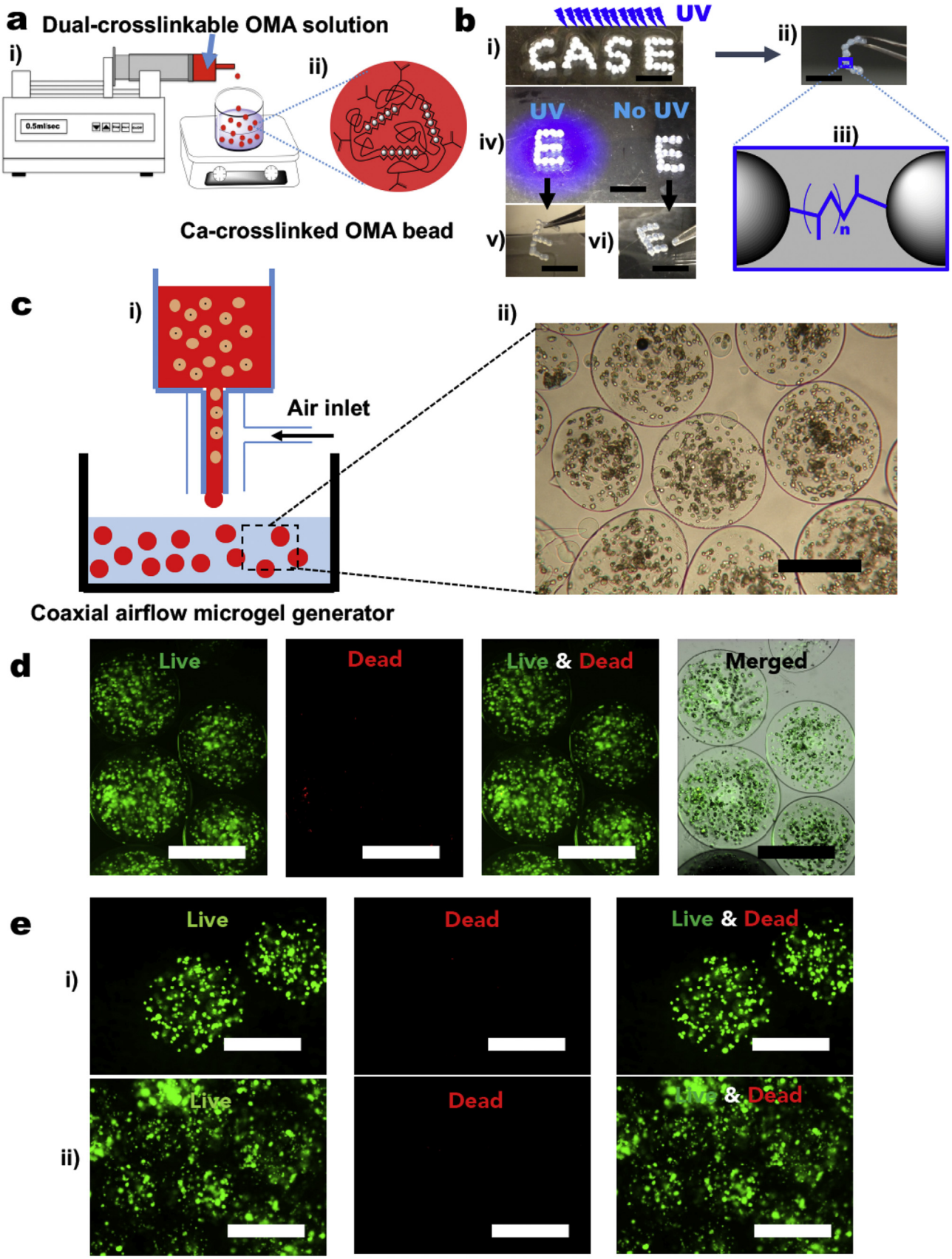

Fig. 1. Fabrication and assembly of the OMA hydrogel beads and hMSC-laden OMA microgels. (a) Schematic depicting (i) OMA bead fabrication and (ii) Ca-crosslinked OMA bead. (b) Fabrication of assembled letters of manually arranged OMA beads connected by photocrosslinking. (i) Ca-crosslinked OMA beads were manually arranged on a glass plate and then assembled under UV light. (ii) Physically linked OMA beads in the letter C were mechanically stable. (iii) Methacrylate groups were photocrosslinked under UV light between the

microgels were labeled with red and green fluorescent dyes, respectively. To prepare the green fluorescent dye solution, 1 ml of FDA solution was mixed with 0.3 ml of PBS (pH 8). Osteogenically differentiated microgels were incubated in the FDA solution for 5 min and then washed with DMEM containing 0.05 w/v % photoinitiator thrice. Chondrogenically differentiated microgels were incubated in 1 ml of PBS (pH 7.4)-contained rhodamine phalloidin (1:200 dilution; Thermo Fisher Scientific) for 60 min and then washed with DMEM containing 0.05 w/v % photoinitiator thrice. Fluorescently labeled microgels were manually heterogeneously assembled and stabilized by photocrosslinking under UV light at 20 mW/cm^2 for 1 min.

2.6. Rheological properties of OMA microgels

Dynamic rheological examination of hMSC-laden OMA microgels was performed to characterize their shear-thinning, self-healing, and mechanical properties with a Haake MARS III rotational rheometer (Thermo Fisher Scientific). Microgel bioink was prepared by mixing hMSC-laden microgels (10 ml) and OMA solution (3 ml, 4 w/v % OMA, which has 9% of actual oxidation and 14% of actual methacrylation degree [30], in DMEM containing 0.05 w/v % photoinitiator), and then excess OMA solution was removed after centrifugation at 500 g with a Sorvall Legend RT Plus Centrifuge. In oscillatory mode, a parallel-plate (80 mm diameter) geometry measuring system was used, and the gap was set to 1 mm. After the sample was placed between the plates, all the tests were started at 37 ± 0.1 °C, and the plate temperature was maintained at 37 °C. An oscillatory frequency sweep (0.01–1.3 Hz; 1% strain) test was performed to measure the storage modulus (G′), the loss modulus (G″), and viscosity. An oscillatory strain sweep (0.1%–100% strain; 1 Hz) test was performed to show the shear-thinning characteristics of the hMSC-laden OMA microgels and to determine the shear-yielding point at which the hMSC-laden OMA microgels behave fluid-like. To demonstrate the self-healing properties of hMSC-laden OMA microgels, a cyclic deformation test was performed at 100% strain with recovery at 1% strain, each for 1 min at 1 Hz.

2.7. Modification of the 3D printer

All 3D printing was performed using a 3D printer modified with a syringe-based extruder [31]. The stock thermoplastic extruder assembly was replaced with a custom-built syringe pump extruder (Fig. 4a). The syringe pump extruder was designed to use the NEMA-17 stepper motor from the original Printrbot thermoplastic extruder and to mount directly in place of the extruder on the *x*-axis carriage. The syringe pump extruder was printed with polylactic acid using the thermoplastic extruder on the Printrbot before its removal. By using the same stepper motor, the syringe pump extruder was natively supported by the software that came with the printer. The design for the syringe pump extruder and the image files of the human femur and skull were downloaded as stereolithography files from the National Institutes of Health 3D Print Exchange (http://3dprint.nih.gov) under an open-source license. Digital image files of letters for 3D printing were generated from www.tinkercad.com. The file for the human ear was downloaded from www.thingiverse.com/thing:304657 under the terms of the Creative Commons Attribution license, which permits unrestricted use, reproduction, and distribution in any medium.

2.8. 3D printing of microgels

For the 3D printing of microgels, the hMSC-suspended OMA solution was pumped at 0.5 ml/s with an outer air flow rate of 15 L/min, and the droplets dripped into a collection bath containing an aqueous solution of $CaCl_2$ (0.2 M). After crosslinking in the bath for 30 min, the resultant hMSC-laden OMA microgels were collected and washed with DMEM thrice. The viability of encapsulated hMSCs in the OMA microgels was investigated as described above. To visualize some of the microgels during printing, microgels were stained with Alizarin red S (2 w/v %) for 30 min, and washed with DMEM thrice. For 3D printing of microgels, microgel bioink was prepared as described earlier. The gelatin slurry for supporting bath was prepared as described previously [31]. hMSC-laden microgel bioink was loaded into a 2.5-ml syringe (Gastight Syringe, Hamilton Company) with 0.5-inch 20G stainless steel needle (McMaster-Carr). The syringe was then mounted into the syringe pump extruder on the 3D printer. A petri dish filled with gelatin slurry at room temperature as a supporting bath was placed on the building platform. The tip of the needle was positioned at the center and near the bottom of the dish. After 3D printing, printed constructs were stabilized by photocrosslinking under UV at 20 mW/cm^2 for 1 min. After photocrosslinking, constructs in the gelatin slurry were transfer into preheated DMEM (38 °C). Once the gelatin slurry was melted, printed constructs were rinsed with preheated DMEM thrice and placed in a humidified incubator at 37 °C with 5% CO_2. The viability of hMSCs in the 3D printed constructs was investigated as described previously.

The hMSC-laden OMA microgels were osteogenically or chondrogenically differentiated in spinner flasks for 4 weeks, and stained with Alizarin Red S (2 w/v % for 5 min) and Toluidine blue O (0.5 w/v % for 30 min), respectively, washed with diH2O thrice, and then used as bioinks. The microgel bioink was prepared and printed into the gelatin slurry as described previously. After photocrosslinking under UV light at 20 mW/cm^2 for 1 min, constructs in the gelatin slurry were transferred into preheated DMEM (38 °C). Once the gelatin slurry was melted, printed constructs were rinsed with preheated DMEM thrice and imaged with a digital camera (iPhone 6s).

3. Results and discussion

To evaluate the feasibility of facile assembly of OMA microgels, OMA hydrogel beads were fabricated first because they are easier to handle and manually manipulate than microgels. OMA macromer solution was extruded through a needle to form OMA droplets into a calcium chloride gelling bath (Fig. 1a, (i)). OMA droplets immediately reacted with Ca^{2+} to form ionically crosslinked OMA beads (Fig. 1a, (ii)). After manually connecting individual OMA beads on a glass plate Fig. 1b, (i)), structures of physically linked OMA beads were fabricated using the application of UV irradiation (Fig. 1b, (ii)). Because the ionically crosslinked OMA beads have methacrylated groups, crosslinks formed under UV light between the OMA bead units to stabilize the resulting assembly (Fig. 1b, (iii)). Although the OMA beads joined together via photocrosslinking could be lifted up

OMA bead units to stabilize the resulting assembly. (iv) Beads were manually arranged to form the letter E on a glass plate. (v) OMA beads joined together via photocrosslinking could be lifted up from the glass plate. (vi) Individual OMA beads detached from non–UV-irradiated OMA bead samples. The scale bars indicate 10 mm. (c) (i) Schematic diagram of coaxial airflow–induced microgel generator and (ii) a representative photograph of hMSC-laden OMA microgels. (d) Live/Dead staining of encapsulated hMSCs in OMA microgels at day 0. Green color indicates vital cells and red color indicates dead cells. (e) Live/Dead images of hMSC-laden microgels after 4 weeks of culture before (i) and after (ii) assembly under UV light. The scale bars indicate 200 μm. OMA, oxidized methacrylated alginate; hMSC, human bone marrow–derived mesenchymal stem cell.

from the glass plate as a stand-alone assembled construct (Fig. 1b, (v)), individual OMA beads detached from a non-UV irradiated OMA bead assembly (Fig. 1b, (vi)). To evaluate the capability of a magnetic assembly approach, which is a robust and facile method to assemble small particles and fabricate various structures, magnetic OMA beads were prepared. As shown in Supplementary Fig. 1, magnetic OMA beads could be assembled into letter, dome, and tube shapes. Although this approach offers simple and rapid assembly of magnetic OMA beads, there is still limited control over the formation of complex, 3D biological structures.

As smaller microgels (diameter <300 μm) can enhance mass transport to/from encapsulated cells to achieve a more efficient nutrient and waste exchange because of larger surface-to-volume ratio [35], alginate beads (diameter > 1 mm) formed by the

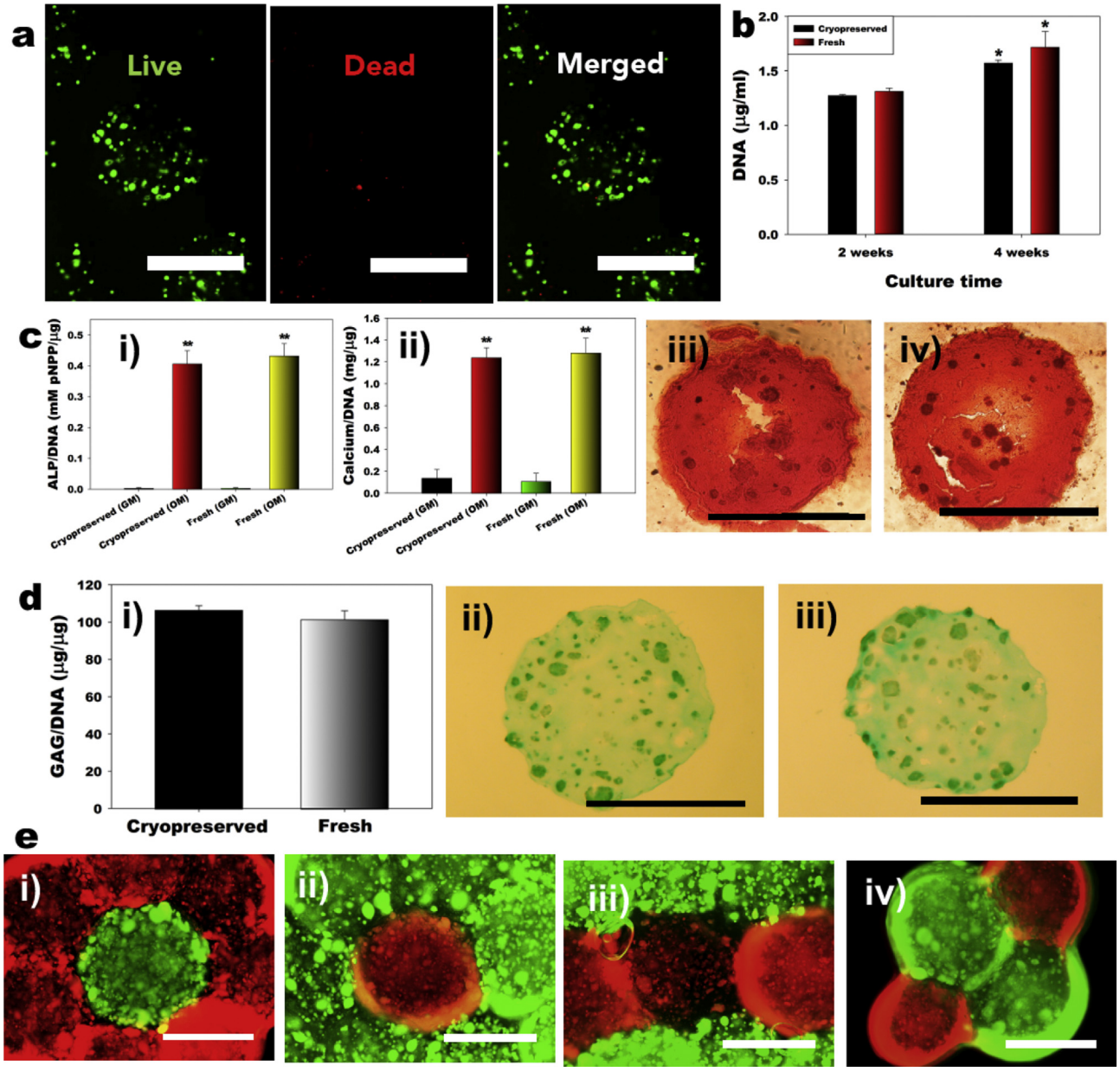

Fig. 2. Cryopreservation of hMSC-laden OMA microgels. (a) Live/Dead images of cryopreserved hMSC-laden OMA microgels after recovery from cryopreservation in liquid nitrogen. Green color indicates vital cells and red color indicates dead cells. (b) Quantification of DNA in the hMSC-laden OMA microgels after 2 weeks and 4 weeks of culture in growth media. $^{*}p < 0.05$ compared with 2 weeks at a specific group. (c) Osteogenic differentiation of cryopreserved hMSC-laden OMA microgels for 4 weeks. Quantification of (i) ALP activity and (ii) mineralization normalized by DNA, and Alizarin red S staining of (iii) freshly made and (iv) cryopreserved hMSC-laden OMA microgels demonstrated no significant differences between cryopreserved and fresh microgels. $^{**}p < 0.05$ compared with Cryopreserved (GM) and Fresh (GM). (d) Chondrogenic differentiation of cryopreserved hMSC-laden OMA microgels for 4 weeks. (i) Quantification of GAG content normalized DNA and Alcian blue staining of (ii) freshly made and (iii) cryopreserved hMSC-laden OMA microgels also demonstrated no significant differences between cryopreserved and fresh microgels. (e) Heterogeneously assembled osteogenically (red) and chondrogenically (green) differentiated hMSC-laden OMA microgels structures. (i) Osteogenically differentiated hMSC-laden OMA microgels were assembled around a chondrogenically differentiated hMSC-laden OMA microgel. (ii) Chondrogenically differentiated hMSC-laden OMA microgels were assembled around an osteogenically differentiated hMSC-laden OMA microgel. (iii) Osteogenically differentiated hMSC-laden OMA microgel layer was assembled between chondrogenically differentiated hMSC-laden OMA microgel layers. (iv) Two of chondrogenically differentiated hMSC-laden OMA microgels were connected. Subsequently, osteogenically differentiated hMSC-laden OMA microgels were attached to the assembly. The scale bars indicate 200 μm. OMA, oxidized methacrylated alginate; hMSC, human bone marrow–derived mesenchymal stem cell; GAG, glycosaminoglycan.

simple dripping method are not ideal for cell encapsulation. Therefore, a coaxial airflow–induced microgel generator was designed (Fig. 1c, (i)) that could fabricate microgels (diameter < 300 μm) with encapsulated hMSC (Fig. 1c, (ii)). High cell viability was observed after cell encapsulation (Fig. 1d), indicating that the macromer solution, coaxial flow, and ionic cross-linking (0.2 M $CaCl_2$) encapsulation process were non-toxic to the cells. Microgel encapsulated hMSCs also maintained high cell viability after 4 weeks of spinner flask culture (Fig. 1e, (i)). Furthermore, these cell-laden microgels could be directly assembled while maintaining high cell viability (Fig. 1e, (ii)).

Because preservation and 'off-the-shelf' availability of biotherapeutics may be valuable for their clinical translation, cryopreservation has been extensively studied as a viable solution to the long-term storage of cells [36], tissues [37], and embryos [38]. The development of effective, safe, and sterile cryopreservation protocols is a prerequisite for the long-term storage of these biologics [39]. DMSO is one of the most commonly used cryoprotectants to aid in the long-term storage of viable biologics because of its ability to penetrate the cell membrane and reduce the formation of ice crystals during the freezing process [40]. As 10% DMSO has been shown to not adversely affect hMSCs' viability and proliferative capacities [41], in this study, a mixture of 10% DMSO and 90% growth medium (DMEM with 10% FBS, 1% P/S, and 10 ng/ml FGF-2) was used as a cryopreservation solution for hMSC-laden microgels. The cryopreserved microgels with encapsulated hMSCs thawed rapidly during the recovery process, and the viability of recovered hMSCs was examined using a live/dead assay. hMSCs exhibited high cell viability after recovery from cryopreservation in liquid nitrogen (Fig. 2a).

Because cryopreservation has been known to affect the function of stem cells [42], the proliferative capacities and differentiation potentials of hMSC-laden microgels derived from cryopreserved or freshly prepared microgels were compared. To indirectly examine the change in the number of hMSCs encapsulated within the microgels, DNA content was measured over a period of 4 weeks of culture in the growth medium (Fig. 2b). The DNA content of both microgel groups significantly increased over the 4 weeks. However, there was no significant difference in the DNA content between the two groups. To investigate the effect of microgel cryopreservation on the differentiation behavior of the stem cells, hMSC-laden microgels derived from cryopreserved or freshly prepared microgels were cultured in osteogenic differentiation media for 4 weeks. Osteogenesis of hMSCs was evaluated by measuring alkaline phosphatase (ALP) activity and quantifying calcium deposition by staining with Alizarin red S (Fig. 2c). ALP activity of encapsulated hMSCs and microgel mineralization were significantly increased by culturing in the osteogenic differentiation medium, compared with the growth medium (Fig. 2c, (i,ii)). However, there was no significant difference in ALP activity (Fig. 2c, (i)) or mineralization (Fig. 2c, (ii-iv)) between cryopreserved and fresh microgels. hMSC-laden microgels derived from cryopreserved or freshly prepared microgels were also cultured in chondrogenic differentiation media for 4 weeks to evaluate the effect of cryopreservation on chondrogenesis of hMSCs encapsulated in microgels. The cell viability of hMSCs in previously cryopreserved microgels was observed to be at a similar level as in fresh microgels after chondrogenic differentiation (Supplementary Fig. 2a). Chondrogenesis of hMSCs was evaluated by quantifying GAG content (Fig. 2d, (i)) and staining with Alcian blue (Fig. 2d, (ii-iii)) and Toluidine blue O (Supplementary Fig. 2b). Similar to the osteogenic differentiation findings, there was no significant difference in GAG/DNA between cryopreserved and fresh microgels (Fig. 2d, (i)). Similar levels of Alcian blue and Toluidine blue O staining was also observed in the cryopreserved

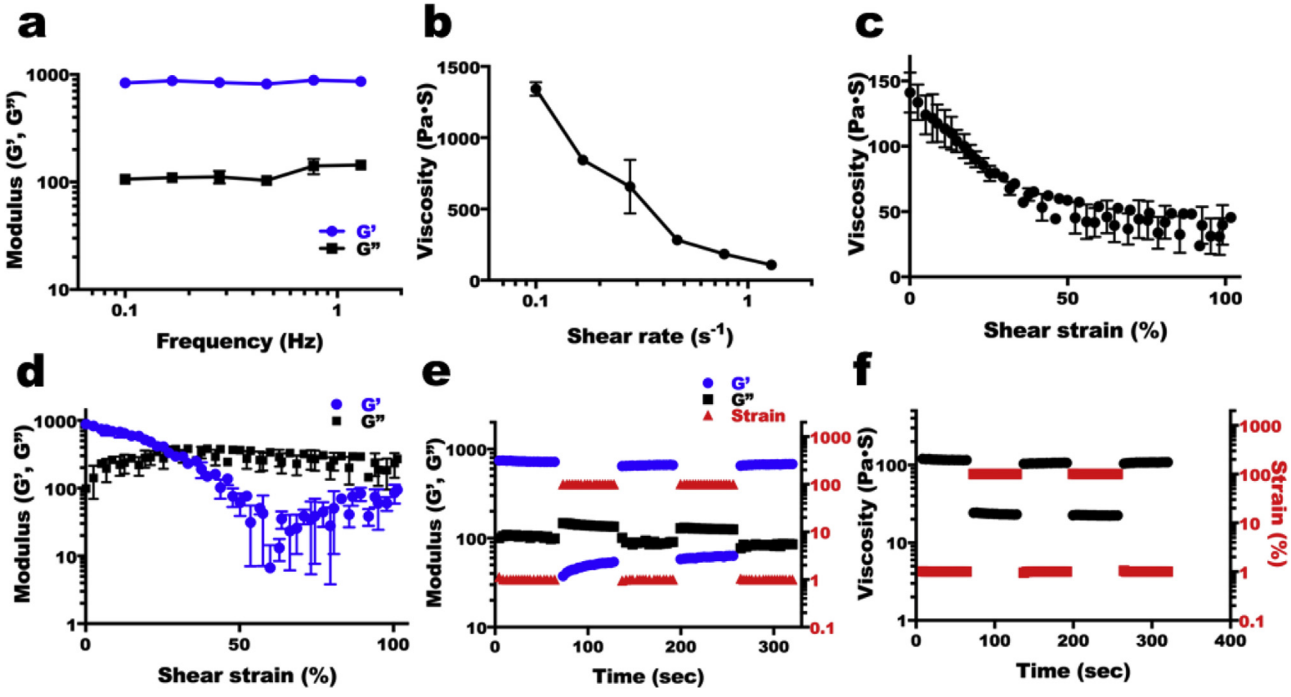

Fig. 3. Shear-thinning and self-healing properties of the OMA microgels. (a) Storage (G′) and loss (G″) moduli of hMSC-laden OMA microgels as a function of frequency. G′ is larger than G″ over the measured frequency range and both exhibited frequency independence. Viscosity of hMSC-laden OMA microgels as a function of (b) shear rate and (c) shear strain demonstrates the shear-thinning behavior of hMSC-laden OMA microgels. (d) G′ and G″ of hMSC-laden OMA microgels as a function of shear strain exhibits their shear-yielding behavior and gel-to-sol transition at higher shear strain. (e) Shear moduli and (f) viscosity changes by dynamic strain tests of hMSC-laden OMA microgels with alternating low (1%) and high (100%) strains at 1 Hz demonstrate rapid recovery of microgel bioink strength and viscosity within seconds, which indicates 'self-healing' or thixotropic properties of hMSC-laden OMA microgels. OMA, oxidized methacrylated alginate; hMSC, human bone marrow–derived mesenchymal stem cell.

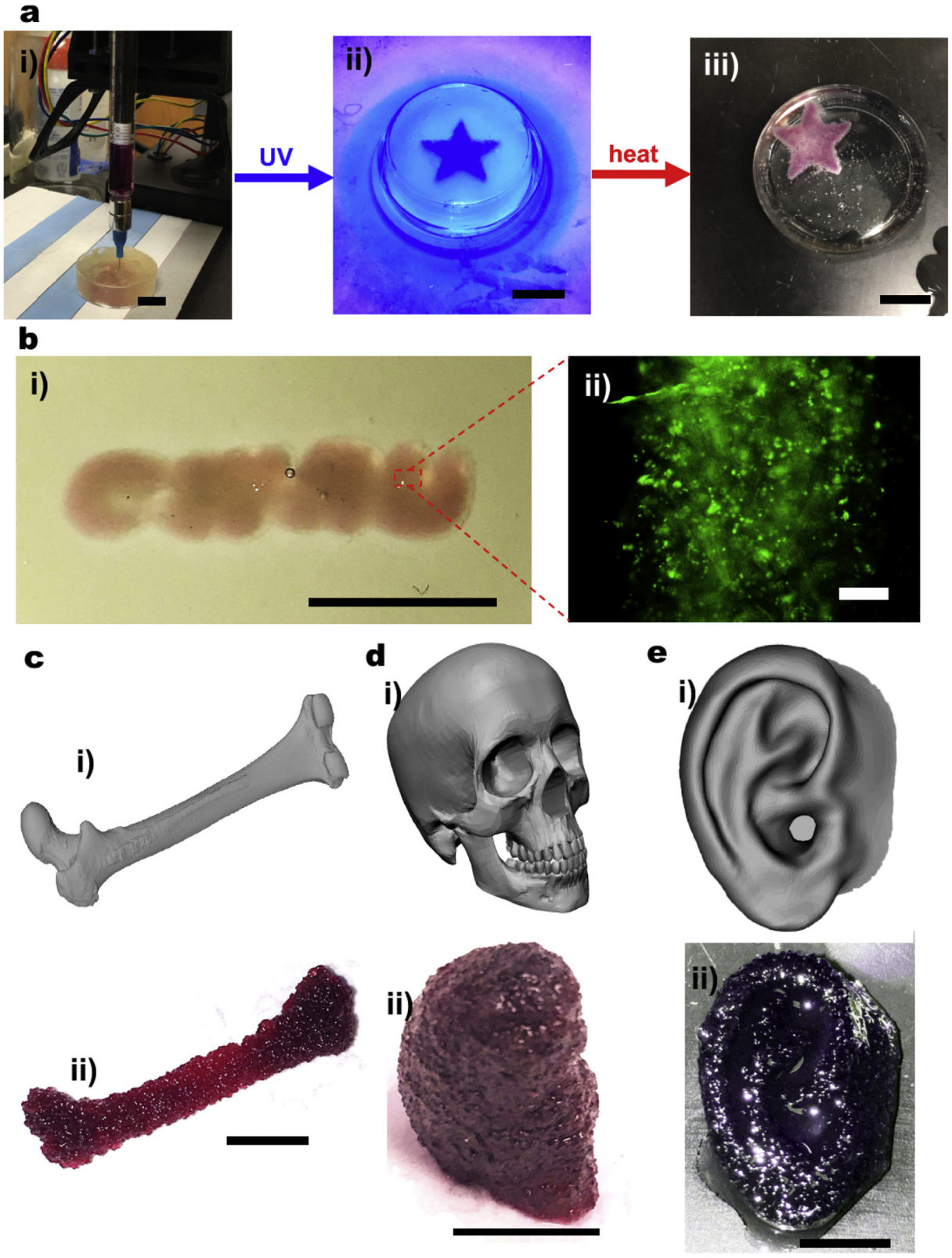

Fig. 4. FRESH 3D printing of hMSC-laden OMA microgels. (a) (i) FRESH 3D printing of Alizarin red S–stained hMSC-laden OMA microgels using a 3D printer modified with a custom syringe-based extruder; (ii) assembly of a 3D printed star-shaped structure by photocrosslinking; (iii) heated release of the assembled structure from the gelatin slurry bath. To visualize the 3D printed structure, microgels were stained with Alizarin red S before printing. (b) (i) FRESH 3D printed letters (CWRU) and (ii) a Live/Dead image of an assembled 3D printed structure. Green color indicates vital cells, and red color indicates dead cells. The 3D printed (c) femur and (d) skull using Alizarin red S–stained hMSC-laden OMA microgels after osteogenic differentiation, and (e) an ear using Toluidine blue O stained hMSC-laden OMA microgels after chondrogenic differentiation. (i) digital images and (ii) 3D printed structures. The black scale bars and the white scale bar indicate 1 cm and 100 μm, respectively. OMA, oxidized methacrylated alginate; hMSC, human bone marrow–derived mesenchymal stem cell; GAG, glycosaminoglycan; FRESH, free-form reversible embedding of suspended hydrogel.

hMSC-laden microgels and fresh microgels. The formation of cell clusters was observed throughout both the groups, further indicating chondrogenic differentiation [43]. These results clearly demonstrate that the differentiation potential of hMSC-laden microgels toward the osteogenic and chondrogenic pathways was maintained even after cryopreservation. Thus, these cryopreserved hMSCs encapsulated in microgels with preserved proliferation and differentiation capabilities could be valuable for tissue regeneration and cell-based therapies. Osteogenically and chondrogenically differentiated OMA microgels, labeled with red and green fluorescent dyes to permit visualization, were then manually heterogeneously assembled, successfully stabilized by photocrosslinking under UV light, and imaged (Fig. 2e). This demonstrates how the microgels can be readily used as building blocks to assemble structures composed of diverse components.

When typical macromer solutions and hydrogels used as bioinks in 3D printing are extruded through a syringe and needle, they become more viscous which makes it challenging to use them in these applications. Shear-thinning and self-healing characteristics can enhance the 3D printing capacity of materials [44,45]; therefore, we evaluated whether the hMSC-laden microgels exhibit these properties before utilizing them for 3D bioprinting. Frequency sweeps of hMSC-laden OMA microgels showed significantly higher G′ than G″, indicating that hMSC-laden OMA microgels were mechanically stable (Fig. 3a). From continuous flow experiments, we observed that the viscosity of hMSC-laden OMA microgel bioink decreased with increasing shear rate and shear strain, demonstrating shear-thinning characteristics (Fig. 3b and c). Moreover, G″ surpassed G′ at approximately 25% strain in an oscillatory strain sweep test, which is an indication of shear-yielding, an important property of hydrogel materials for injectability and/or printability through a needle (Fig. 3d). When investigated under the cyclic strain sweeps by alternating low (1%) and high (100%) strains, the hMSC-laden OMA microgel bioink went from solid-like to liquid-like behavior in response to strain (Fig. 3e). Furthermore, the responses of shear moduli (Fig. 3e) and viscosity (Fig. 3f) to high strain and recoveries at low strain were rapid and repeatable. The combination of shear-thinning and shear-yielding properties allows for the rapid transition from solid-like to liquid-like behavior, making the hMSC-laden OMA microgels well suited for injection and extrusion-based 3D printing. The rapid recovery of mechanical properties after removal of shear force, as occurs after the deposition of the OMA microgel bioink, allows for stabilization of the printed bioink immediately after extrusion.

The potential of hMSC-laden OMA microgels to serve as a bioink to form complex 3D printed biological structures using the FRESH 3D bioprinting technique was then examined [31]. Here, we show that hMSC-laden microgel bioink could be printed by extrusion within the gelatin microparticle slurry support bath (Supplementary Fig. 4b), which maintains the intended 3D printed structure during the printing process (Fig. 4a, (i) and Supplementary Fig. 4a). After the entire 3D structure was printed, hMSC-laden microgels were crosslinked together under UV light (Fig. 4a, (ii)). By incubating the 3D printed structure at 37 °C, the supporting gelatin bath could be easily removed in a non-destructive manner (Fig. 4a, (iii)). As shown in Fig. 4b (letters of CWRU), high cell viability was observed even after 3D printing and removal of the gelatin slurry, indicating that the FRESH 3D printing of cryopreserved microgels is a cell-friendly process. To demonstrate construction of tissue constructs with complex shapes, a femur (Fig. 4c), a skull (Fig. 4d), an ear (Fig. 4e), letters (Supplementary Fig. 4c), and a cube (Supplementary Fig. 4d) were fabricated using 3D printing of the osteogenically or chondrogenically differentiated hMSC-laden microgels. Upon FRESH 3D bioprinting and assembly of Alizarin red S stained− (femur and skull) and Toluidine blue O stained−microgels (ear), it was demonstrated that stem cell−laden microgels differentiated down that specific lineages could be applied using this strategy to create biological complex structures.

4. Conclusion

hMSC-laden microgels have been fabricated using an ionically crosslinked OMA hydrogel. The hMSC-laden OMA microgels were directly assembled into well-defined, complicated 3D shapes and structures via photopolymerization. hMSC-laden OMA microgels were successfully cryopreserved for long-term storage and off-the-shelf availability, and hMSCs in thawed microgels had equivalent functionality compared with freshly processed stem cells. Finally, cell-laden OMA microgels could be applied as a unique bioink for FRESH bioprinting to create complex 3D tissue structures. The directed assembly and 3D printing of stem cell−laden OMA microgels provide a powerful and highly scalable platform technology for biomimetic 3D tissue construction and present a new paradigm for 3D bioprinting of microscale materials.

Author contributions

O.J. and E.A. conceived the ideas and designed the experiments. O.J. and Y.B.L. conducted the experiments. O.J., Y.B.L., and E.A. analyzed and interpreted the data. O.J., Y.B.L., T.J.H., A.W.F., and E.A. wrote and/or reviewed the manuscript.

Competing financial interests

T.J.H and A.W.F have an equity stake in FluidForm, LLC, which is a startup company commericializing FRESH 3D printing. FRESH 3D printing is the subject of patent protection including UP Patent number 10,150,258 and others.

Data availability statement

The data sets generated and/or analyzed during the present study are available from the corresponding author upon reasonable request.

Acknowledgments

The authors thank Kee-Won Lee for assistance in preparation of gelatin hydrogel slurry. The authors gratefully acknowledge funding from the National Institutes of Health's National Institute of Arthritis and Musculoskeletal and Skin Diseases (R01AR069564, R01AR066193; E.A.) and National Heart, Lung, and Blood Institute (DP2HL117750; A.W.F.). The contents of this publication are solely the responsibility of the authors and do not necessarily represent the official views of the National Institutes of Health.

Appendix A. Supplementary data

Supplementary data to this article can be found online at https://doi.org/10.1016/j.mtchem.2018.11.009.

References

[1] L.M. Calvi, G.B. Adams, K.W. Weibrecht, J.M. Weber, D.P. Olson, M.C. Knight, R.P. Martin, E. Schipani, P. Divieti, F.R. Bringhurst, L.A. Milner, H.M. Kronenberg, D.T. Scadden, Osteoblastic cells regulate the haematopoietic stem cell niche, Nature 425 (6960) (2003) 841−846.

[2] S.D. McCullen, H. Autefage, A. Callanan, E. Gentleman, M.M. Stevens, Anisotropic fibrous scaffolds for articular cartilage regeneration, Tissue Eng. Part A 18 (19−20) (2012) 2073−2083.

[3] C.M. Nelson, M.J. Bissell, Modeling dynamic reciprocity: engineering three-dimensional culture models of breast architecture, function, and neoplastic transformation, Semin. Canc. Biol. 15 (5) (2005) 342–352.
[4] A. Khademhosseini, R. Langer, A decade of progress in tissue engineering, Nat. Protoc. 11 (10) (2016) 1775–1781.
[5] A. Khademhosseini, J.P. Vacanti, R. Langer, Progress in tissue engineering, Sci. Am. 300 (5) (2009) 64–71.
[6] C.W. Cheng, L.D. Solorio, E. Alsberg, Decellularized tissue and cell-derived extracellular matrices as scaffolds for orthopaedic tissue engineering, Biotechnol. Adv. 32 (2) (2014) 462–484.
[7] A. Khademhosseini, R. Langer, J. Borenstein, J.P. Vacanti, Microscale technologies for tissue engineering and biology, Proc. Natl. Acad. Sci. USA 103 (8) (2006) 2480–2487.
[8] R. Langer, Editorial: tissue engineering: perspectives, challenges, and future directions, Tissue Eng. 13 (1) (2007) 1–2.
[9] V. Mironov, R.P. Visconti, V. Kasyanov, G. Forgacs, C.J. Drake, R.R. Markwald, Organ printing: tissue spheroids as building blocks, Biomaterials 30 (12) (2009) 2164–2174.
[10] D.L. Elbert, Bottom-up tissue engineering, Curr. Opin. Biotechnol. 22 (5) (2011) 674–680.
[11] J.W. Nichol, A. Khademhosseini, Modular tissue engineering: engineering biological tissues from the bottom up, Soft Matter 5 (7) (2009) 1312–1319.
[12] A. Leferink, D. Schipper, E. Arts, E. Vrij, N. Rivron, M. Karperien, K. Mittmann, C. van Blitterswijk, L. Moroni, R. Truckenmuller, Engineered micro-objects as scaffolding elements in cellular building blocks for bottom-up tissue engineering approaches, Adv. Mater. 26 (16) (2014) 2592–2599.
[13] J.S. Liu, Z.J. Gartner, Directing the assembly of spatially organized multicomponent tissues from the bottom up, Trends Cell Biol. 22 (12) (2012) 683–691.
[14] B.V. Slaughter, S.S. Khurshid, O.Z. Fisher, A. Khademhosseini, N.A. Peppas, Hydrogels in regenerative medicine, Adv. Mater. 21 (32–33) (2009) 3307–3329.
[15] J.L. Drury, D.J. Mooney, Hydrogels for tissue engineering: scaffold design variables and applications, Biomaterials 24 (24) (2003) 4337–4351.
[16] A.P. McGuigan, M.V. Sefton, Vascularized organoid engineered by modular assembly enables blood perfusion, Proc. Natl. Acad. Sci. USA 103 (31) (2006) 11461–11466.
[17] M. Chen, X. Wang, Z. Ye, Y. Zhang, Y. Zhou, W.S. Tan, A modular approach to the engineering of a centimeter-sized bone tissue construct with human amniotic mesenchymal stem cells-laden microcarriers, Biomaterials 32 (30) (2011) 7532–7542.
[18] S.E. Chung, W. Park, S. Shin, S.A. Lee, S. Kwon, Guided and fluidic self-assembly of microstructures using railed microfluidic channels, Nat. Mater. 7 (7) (2008) 581–587.
[19] S.E. Chung, Y. Jung, S. Kwon, Three-dimensional fluidic self-assembly by axis translation of two-dimensionally fabricated microcomponents in railed microfluidics, Small 7 (6) (2011) 796–803.
[20] Y.A. Du, M. Ghodousi, E. Lo, M.K. Vidula, O. Emiroglu, A. Khademhosseini, Surface-directed assembly of cell-laden microgels, Biotechnol. Bioeng. 105 (3) (2010) 655–662.
[21] F. Xu, T.D. Finley, M. Turkaydin, Y.R. Sung, U.A. Gurkan, A.S. Yavuz, R.O. Guldiken, U. Demirci, The assembly of cell-encapsulating microscale hydrogels using acoustic waves, Biomaterials 32 (31) (2011) 7847–7855.
[22] N.N. Kachouie, Y.A. Du, H. Bae, M. Khabiry, A.F. Ahari, B. Zamanian, J. Fukuda, A. Khademhosseini, Directed assembly of cell-laden hydrogels for engineering functional tissues, Organogenesis 6 (4) (2010) 234–244.
[23] V.L. Tsang, A.A. Chen, L.M. Cho, K.D. Jadin, R.L. Sah, S. DeLong, J.L. West, S.N. Bhatia, Fabrication of 3D hepatic tissues by additive photopatterning of cellular hydrogels, Faseb. J. 21 (3) (2007) 790–801.
[24] Y. Du, E. Lo, S. Ali, A. Khademhosseini, Directed assembly of cell-laden microgels for fabrication of 3D tissue constructs, Proc. Natl. Acad. Sci. U. S. A. 105 (28) (2008) 9522–9527.
[25] S.V. Murphy, A. Atala, 3D bioprinting of tissues and organs, Nat. Biotechnol. 32 (8) (2014) 773–785.
[26] B. Derby, Printing and prototyping of tissues and scaffolds, Science 338 (6109) (2012) 921–926.
[27] N.E. Fedorovich, J.R. De Wijn, A.J. Verbout, J. Alblas, W.J. Dhert, Three-dimensional fiber deposition of cell-laden, viable, patterned constructs for bone tissue printing, Tissue Eng. Part A 14 (1) (2008) 127–133.
[28] H.W. Kang, S.J. Lee, I.K. Ko, C. Kengla, J.J. Yoo, A. Atala, A 3D bioprinting system to produce human-scale tissue constructs with structural integrity, Nat. Biotechnol. 34 (3) (2016) 312–319.
[29] X. Wang, Y. Yan, R. Zhang, Recent trends and challenges in complex organ manufacturing, Tissue Eng. B Rev. 16 (2) (2010) 189–197.
[30] O. Jeon, D.S. Alt, S.M. Ahmed, E. Alsberg, The effect of oxidation on the degradation of photocrosslinkable alginate hydrogels, Biomaterials 33 (13) (2012) 3503–3514.
[31] T.J. Hinton, Q. Jallerat, R.N. Palchesko, J.H. Park, M.S. Grodzicki, H.J. Shue, M.H. Ramadan, A.R. Hudson, A.W. Feinberg, Three-dimensional printing of complex biological structures by freeform reversible embedding of suspended hydrogels, Sci. Adv. 1 (9) (2015) e1500758.
[32] O. Jeon, D.W. Wolfson, E. Alsberg, In-situ formation of growth-factor-loaded coacervate microparticle-embedded hydrogels for directing encapsulated stem cell fate, Adv. Mater. 27 (13) (2015) 2216–2223.
[33] D.P. Lennon, S.E. Haynesworth, S.P. Bruder, N. Jaiswal, A.I. Caplan, Human and animal mesenchymal progenitor cells from bone marrow: identification of serum for optimal selection and proliferation, In Vitro Cell Dev.-An. 32 (10) (1996) 602–611.
[34] O. Jeon, E. Alsberg, Regulation of stem cell fate in a three-dimensional micropatterned dual-crosslinked hydrogel system, Adv. Funct. Mater. 23 (38) (2013) 4765–4775.
[35] W.Q. Jiang, M.Q. Li, Z.Z. Chen, K.W. Leong, Cell-laden microfluidic microgels for tissue regeneration, Lab a Chip 16 (23) (2016) 4482–4506.
[36] H. Baharvand, G.H. Salekdeh, A. Taei, S. Mollamohammadi, An efficient and easy-to-use cryopreservation protocol for human ES and iPS cells, Nat. Protoc. 5 (3) (2010) 588–594.
[37] Y.C. Song, B.S. Khirabadi, F. Lightfoot, K.G.M. Brockbank, M.J. Taylor, Vitreous cryopreservation maintains the function of vascular grafts, Nat. Biotechnol. 18 (3) (2000) 296–299.
[38] K. Oktay, Further evidence on the safety and success of ovarian stimulation with letrozole and tamoxifen in breast cancer patients undergoing in vitro fertilization to cryopreserve their embryos for fertility preservation, J. Clin. Oncol. 23 (16) (2005) 3858–3859.
[39] J. Pacchiarotti, T. Ramos, K. Howerton, S. Greilach, K. Zaragoza, M. Olmstead, F. Izadyar, Developing a clinical-grade cryopreservation protocol for human testicular tissue and cells, BioMed Res. Int. 2013 (2013) 930962.
[40] J.O.M. Karlsson, E.G. Cravalho, I.H.M.B. Rinkes, R.G. Tompkins, M.L. Yarmush, M. Toner, Nucleation and growth of ice crystals inside cultured-hepatocytes during freezing in the presence of dimethyl-sulfoxide, Biophys. J. 65 (6) (1993) 2524–2536.
[41] C.J. Hunt, Cryopreservation of human stem cells for clinical application: a Review, Transfus. Med. Hemotherapy 38 (2) (2011) 107–123.
[42] D. Berz, E.M. McCormack, E.S. Winer, G.A. Colvin, P.J. Quesenberry, Cryopreservation of hematopoietic stem cells, Am. J. Hematol. 82 (6) (2007) 463–472.
[43] Y.W. Ewa-Choy, B. Pingguan-Murphy, N.A. Abdul-Ghani, J. Jahendran, K.H. Chua, Effect of alginate concentration on chondrogenesis of co-cultured human adipose-derived stem cells and nasal chondrocytes: a biological study, Biomater. Res. 21 (2017) 19.
[44] L.L. Ouyang, C.B. Highley, C.B. Rodell, W. Sun, J.A. Burdick, 3D printing of shear-thinning hyaluronic acid hydrogels with secondary cross-linking, ACS Biomater. Sci. Eng. 2 (10) (2016) 1743–1751.
[45] C. Loebel, C.B. Rodell, M.H. Chen, J.A. Burdick, Shear-thinning and self-healing hydrogels as injectable therapeutics and for 3D-printing, Nat. Protoc. 12 (8) (2017) 1521–1541.